Spatio-temporal behavior of magnetohydrodynamic fluctuations with cross-helicity and background magnetic field

R. Lugones,[1, a)] P. Dmitruk,[1] P.D. Mininni,[1] A. Pouquet,[2] and W.H. Matthaeus[3]
[1)] *Departamento de Física, Facultad de Ciencias Exactas y Naturales, Universidad de Buenos Aires and IFIBA, CONICET, Ciudad Universitaria, 1428 Buenos Aires, Argentina.*
[2)] *National Center for Atmospheric Research, CISL, NCAR, UCAR, CO , USA*
[3)] *Bartol Research Institute and Department of Physics and Astronomy, University of Delaware, Newark, DE 19716, USA.*

In this work we study the spatio-temporal behavior of the Elsässer variables describing magnetic and velocity field fluctuations, using direct numerical simulations of three-dimensional magnetohydrodynamic turbulence. We consider cases with relatively small, intermediate, and large values of a mean background magnetic field, and with null, small, and high cross-helicity. Wavenumber-dependent time correlation functions are computed for the different simulations, varying the mean magnetic field intensity as well as the cross-helicity in the flow. From these correlation functions, the decorrelation time is computed and compared with different theoretical characteristic times: the local non-linear time, the random-sweeping time, and the Alfvénic time. It is found that decorrelation times are dominated by sweeping effects for low values of the mean magnetic field and for low values of the cross-helicity, while for large values of the background field or of the cross-helicity and for wave vectors sufficiently aligned with the guide field, decorrelation times are controlled by Alfvénic effects. Finally, we observe counter-propagation of Alfvénic fluctuations due to reflections produced by inhomogeneities in the total magnetic field. This effect becomes more prominent in flows with large cross-helicity, strongly modifying the propagation of waves in turbulent magnetohydrodynamic flows.

I. INTRODUCTION

Turbulent fluctuations are essentially broadband, both in spatial and temporal scales, involving non-linear couplings among a wide range of scales[1]. In incompressible magnetohydrodynamics (MHD)[2,3] these couplings are based on interactions of triads of modes[4,5] which can be of different types, such as (local in wavenumber space) nonlinear distortions of eddies, or (non-local in wavenumber space) sweeping of small eddies by larger ones[6–12]. Of course, these non-linear couplings also involve interactions with waves in the flow, which are ubiquitous in MHD flows as well as in plasma turbulence.

When linearized, the incompressible MHD equations sustain Alfvén waves, which in the presence of a background magnetic field $\mathbf{B}_0'$ are described by a linear dispersion relation of frequency $\omega = \mathbf{k} \cdot \mathbf{V}_\mathrm{A}$ for the wavevector $\mathbf{k}$, with Alfvén velocity $\mathbf{V}_\mathrm{A} = \mathbf{B}_0'/\sqrt{4\pi\rho}$ and with mass density ρ. It is well known that these waves, when considered in isolation, are also exact solutions of the non-linear MHD (ideal) equations. Simultaneous presence of counter-propagating fluctuations however activate non-linear interactions among modes, producing dispersion, and in consequence the waves are no longer exact solutions of the system[13]. As the background magnetic field controls the wave velocity (i.e., the Alfvén velocity), the non-linear interaction is influenced by the Alfvén crossing time of counter-propagating wave packets. There is therefore a competence between non-linear interactions (i.e., turbulence) and wave propagation[14].

The strength of counter-propagating fluctuations can be measured by the cross-helicity, a quantity which is a quadratic invariant of the ideal MHD equations (see Sec. II for specifics). This quantity is also of relevance for the solar wind and for space plasmas, as large-scale flows with cross-helicity (in the presence of a guide field) are often found in the interplanetary medium. A spatio-temporal analysis of field fluctuations[11,15] can thus be performed to quantitatively study the importance of these different effects, and to distinguish which is the dominant timescale among the different ones depending on the controlling parameters of the system. This kind of analysis was performed in the past for MHD flows without cross-helicity[16–18], observing different behaviors depending on whether the turbulence is weak or strong, and a combination of different timescales including a dominance of the sweeping time as the flow decorrelation time when turbulence is strong. However, the effect of changing the strength of counter-propagating fluctuations in the spatio-temporal behavior of the flow, and in its decorrelation time, was not considered before.

In the present paper we perform a spatio-temporal analysis of MHD turbulence, controlling simultaneously the intensity of the background magnetic field and the amount of cross-helicity in the flow, extending our previous study[17] of incompressible MHD with a background magnetic field and no cross-helicity. We present several numerical solutions of the incompressible MHD equations in a turbulent steady state, and analyze each timescale in the system using wavenumber-dependent time correlation functions, and spatio-temporal spectra of the Elsässer variables. The spatio-temporal study of the Elsässer variables allows us to disentangle the two possible polarizations of the Alfvén waves, as well as their

[a)] Electronic mail: rlugones@df.uba.ar

direction of propagation, and to quantify any imbalance between the two polarizations. We find that decorrelation times are dominated by sweeping effects for low values of the mean magnetic field and for low values of the cross-helicity, while for large values of the background field or of the cross-helicity decorrelation times are controlled by the Alfvénic times. Moreover, for large values of the cross-helicity we also observe counter-propagation of Alfvénic fluctuations (i.e., an inversion in the direction of propagation of one polarization of Alfvén waves), resulting from reflections in inhomogeneities of the total magnetic field produced by the turbulence. Under some conditions, this can result in the propagation of both polarizations of the Alfvén waves in the same direction. This effect strongly affects the propagation of waves in turbulent MHD flows, and therefore, non-linear interactions.

The structure of the paper is as follows. In Sec. II we introduce the equations and the numerical methods employed, as well as a description of the spatio-temporal spectrum and of the correlation functions. Results are presented in Sec. III. Finally, discussions and conclusions are presented in Sec. IV.

II. EQUATIONS AND NUMERICAL SIMULATIONS

A. The MHD equations and the Elsässer fields

The incompressible MHD equations (momentum and induction equations) in dimensionless units are

$$\frac{\partial \mathbf{v}}{\partial t} + \mathbf{v}\cdot\nabla\mathbf{v} = -\frac{1}{\rho}\nabla p + \mathbf{j}\times\mathbf{B} + \frac{1}{R}\nabla^2\mathbf{v}, \qquad (1)$$

$$\frac{\partial \mathbf{b}}{\partial t} = \nabla\times(\mathbf{v}\times\mathbf{B}) + \frac{1}{R_m}\nabla^2\mathbf{b}, \qquad (2)$$

where $\mathbf{v}$ is the plasma bulk velocity, and $\mathbf{B} = \mathbf{b} + \mathbf{B}_0$ is the total magnetic field (in units of an Alfvénic speed, and obtained from the total magnetic field $\mathbf{B}'$ in Gaussian units after dividing by $\sqrt{4\pi\rho}$, where ρ is the plasma density). The total magnetic field has a fluctuating part $\mathbf{b}$, and a mean DC field $\mathbf{B}_0 = B_0\hat{\mathbf{x}}$. Finally, $\mathbf{j} = \nabla\times\mathbf{b}$ is the current density, and p is the pressure. The units are based on a characteristic speed v_0, which for MHD is chosen to be the typical Alfvén speed of the magnetic field fluctuations, $v_0 = \sqrt{\langle b^2\rangle/(4\pi\rho)}$, where $\langle.\rangle$ denotes a spatial average. The dimensionless parameters appearing in the equations are the kinetic and magnetic Reynolds numbers, $R = v_0 L/\nu$ and $R_m = v_0 L/\mu$ respectively, with ν the kinematic viscosity, μ the magnetic diffusivity and L the characteristic length scale (the simulation box side length is defined as $2\pi L$). The unit time is $t_0 = L/v_0$, which for MHD becomes the Alfvén crossing time based on magnetic field fluctuations. The Elsässer fields are then defined as

$$\mathbf{z}^{\pm} = \mathbf{v} \pm \mathbf{b}. \qquad (3)$$

In terms of the Elsässer fields, the MHD equations can be written[11] as

$$\partial_t\mathbf{z}^{\pm} = \pm\mathbf{V}_{\rm A}\cdot\nabla\mathbf{z}^{\pm} - \mathbf{z}^{\mp}\cdot\nabla\mathbf{z}^{\pm} - \nabla P + \frac{1}{R}\nabla^2\mathbf{z}^{\pm}, \quad (4)$$

with $P = p/\rho$, and with the assumption that $R = R_m$. In the r.h.s. of Eq. (4) we explicitly separated the convective term into a linear part describing Alfvénic propagation with $\mathbf{V}_{\rm A} = \mathbf{B}_0$ the Alfvén velocity based on the background magnetic field (with $\mathbf{B}_0$ the field in units of velocity), and the non-linear part describing the interaction among counter-propagating wave-like fluctuations. It is evident from this equation that both Elsässer fields must be present to activate the non-linear interactions.

The ideal invariants (i.e., with zero viscosity and resistivity) of incompressible MHD theory can be written in terms of the Elsässer fields. The total energy E (kinetic plus magnetic) in terms of these variables is

$$E = \frac{1}{2}\int\left(|\mathbf{v}|^2 + |\mathbf{b}|^2\right)dV = \frac{1}{4}\int\left(\left|\mathbf{z}^+\right|^2 + \left|\mathbf{z}^-\right|^2\right)dV, \qquad (5)$$

while the cross-helicity H_c is

$$H_c = \int\mathbf{v}\cdot\mathbf{b}\,dV = \frac{1}{4}\int\left(\left|\mathbf{z}^+\right|^2 - \left|\mathbf{z}^-\right|^2\right)dV. \qquad (6)$$

The ratio $\sigma = H_c/E$ measures the amount of counter-propagating fluctuations in the system. A value $\sigma = \pm 1$ corresponds to only one type of fluctuations $\mathbf{z}^{\pm}$, while $\sigma = 0$ represents equipartition between both fields.

Following the works of Matthaeus *et al.*[19] and Zhou *et al.*[20], the ideal MHD equations can be linearized considering the presence of an inhomogeneous background magnetic field and/or an inhomogeneous background flow, as

$$\partial_t\mathbf{z}^{\pm} + \left(L^{\pm}_{\mathbf{x}} + L^{\pm}\right)\mathbf{z}^{\pm} + M^{\pm}_{ik}\mathbf{z}^{\mp}_k = 0, \qquad (7)$$

The linear operators $L^{\pm}_{\mathbf{x}}$, $L^{\pm}$, and $M^{\pm}_{ik}$ involve gradients acting on both the large- and the small-scale fields, and are given by

$$L^{\pm}_{\mathbf{x}} = (\mathbf{U}\mp\mathbf{V}_{\rm A})\cdot\nabla, \qquad (8)$$

$$L^{\pm} = \frac{1}{2}\nabla\cdot\left(\frac{\mathbf{U}}{2}\pm\mathbf{V}_{\rm A}\right), \qquad (9)$$

and

$$M^{\pm}_{ik} = \nabla_k U_i \pm \frac{1}{\sqrt{4\pi\rho}}\nabla_k B'_i - \frac{1}{2}\delta_{ik}\nabla\cdot\left(\frac{\mathbf{U}}{2}\pm\mathbf{V}_{\rm A}\right), \quad (10)$$

where $\mathbf{U}$ is a background flow. Here, both $\mathbf{U}$ and $\mathbf{V}_{\rm A}$ can include large-scale inhomogeneities (including, for $\mathbf{V}_{\rm A}$, inhomogeneities associated to density fluctuations). The mixing terms (those involving the $M^{\pm}_{ik}$ operators) allow the possibility of creating counter propagating fluctuations out of a single-sign propagating fluctuation, by means of reflections due to inhomogeneities in any of the

background fields[21]. In this sense, even if the system starts from an initial condition with only one sign of propagating fluctuations, the reflections by inhomogeneous background fields will create an amount of counter propagating fluctuations which will turn on non-linearities, producing dispersion and turbulence[22,23]. But this effect can also result, in flows with both polarizations of Afvenic excitations, in the counter-propagation of one of the excitations, as will be shown from numerical data in Sec. III.

B. Wavenumber-frequency spectrum and correlation functions

Using scaling arguments, different characteristic times in the system can be estimated. The local eddy turnover time or isotropic non-linear timescale can be defined as $\tau_{nl} \sim 1/[kv(k)]$, where $v(k)$ is the amplitude of the velocity fluctuations at scale $\sim 1/k$. Considering a Kolmogorov-type scaling $v(k) \sim v_{rms}\,(kL)^{-1/3}$, the non-linear time in the inertial range can be written as

$$\tau_{nl} = C_{nl}\left[v_{rms}L^{-1/3}\left(\sqrt{k_\perp^2+k_\parallel^2}\right)^{2/3}\right]^{-1}, \qquad (11)$$

where C_{nl} is a dimensionless constant of order one, and $k_\parallel$ and $k_\perp$ denote the wavenumbers parallel and perpendicular to the background magnetic field. Here, $v_{rms} = \left\langle|\mathbf{v}|^2\right\rangle^{1/2}$ is a global quantity, dominated by contributions from the large scales[3,24].

Another time decorrelation effect is governed by the sweeping characteristic time, which at the scale $\sim 1/k$ can be expressed as

$$\tau_{sw} = C_{sw}\left(v_{rms}\sqrt{k_\perp^2+k_\parallel^2}\right)^{-1}. \qquad (12)$$

This time corresponds to the advection of small-scale structures by the large-scale flow. Finally, a characteristic Alfvén time can be defined as

$$\tau_A = C_A\left(v_A k_\parallel\right)^{-1}. \qquad (13)$$

In the last two expressions, C_{sw} and C_A also are dimensionless constants of order unity.

To disentangle these time scales in the flow, and to identify which is the relevant time scale at a given spatial scale, two tools can be used: the statistical properties of the correlation function in space and time, and the wavenumber-frequency spectrum. We start by introducing the former. The statistics of the Elsässer fields can be characterized by the spatio-temporal two-point autocorrelation function[11]

$$R^\pm(\mathbf{r},\tau) = \left\langle \mathbf{z}^\pm(\mathbf{x},t)\cdot\mathbf{z}^\pm(\mathbf{x}+\mathbf{r},t+\tau)\right\rangle \Big/ \left\langle\left|\mathbf{z}^\pm\right|^2\right\rangle. \qquad (14)$$

The Fourier transform in $\mathbf{r}$ leads to a time-lagged spectral density which can be further factorized as $S(\mathbf{k},\tau) = S(\mathbf{k})\Gamma(\mathbf{k},\tau)$. The function $\Gamma(\mathbf{k},\tau)$ is the scale-dependent correlation function[25–27] which describes the time decorrelation of each spatial mode $\mathbf{k}$, that is, the loss of memory of fluctuations with characteristics lengths of order k_x^{-1}, k_y^{-1}, and k_z^{-1}.

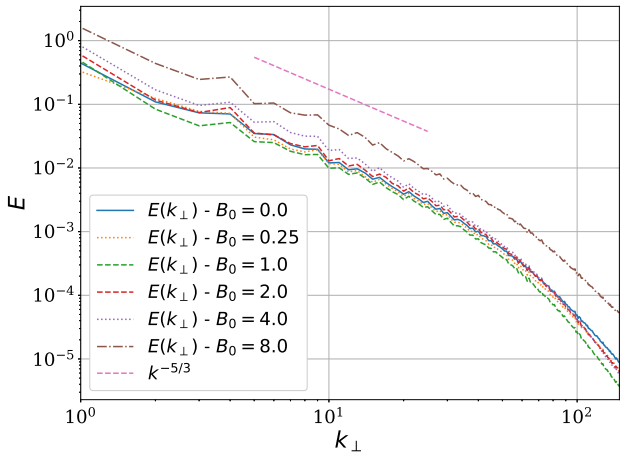

FIG. 1. Reduced perpendicular energy spectra $E(k_\perp)$ for simulations with $B_0 = 0$, 0.25, 1, 2, 4, and 8. All curves correspond to the case $H_c = 0.3$, but the cases with $H_c = 0$ and 0.9 show the same behavior. Kolmogorov scaling, $\sim k_\perp^{-5/3}$, is shown as reference.

When there is a preferential direction in the flow (as in the present case of MHD turbulence with a guide magnetic field), it is useful to assume axial symmetry in Fourier space and to write $\Gamma(\mathbf{k},\tau) = \Gamma(k_\perp,k_\parallel,\tau)$. As this function is three dimensional, it is also useful to study $\Gamma(k_\perp,k_\parallel,\tau)$ with one of the arguments fixed; for instance, fixing a value of $k_\perp$ and analyzing $\Gamma(k_\perp,k_\parallel,\tau)$ as a function of $k_\parallel$ and τ gives us information on fluctuations that vary only in the parallel direction, and allow us to distinguish between decorrelation arising from Alfvénic non-linear interactions or sweeping.

The Fourier transform in the time lag of the scale-dependent correlation function results in the wavenumber-frequency spectrum $E^\pm(\mathbf{k},\omega)$[15,28], for each of the Elsässer fields. These spectra allow identification of modes satisfying the dispersion relation of the system, and provide a direct measurement of how much energy is in those modes, and of how much energy is in other modes. For the two separate Elsässer fields, from Eqs. (5) and (6) it is easy to see that

$$E = E^+ + E^-, \quad H_c = E^+ - E^-, \qquad (15)$$

where $E^\pm = \int|\mathbf{z}^\pm|^2/4\,dV$. Thus, for the wavenumber-frequency spectra of the Elsässer fields, the two following relations hold

$$E^+(\mathbf{k},\omega) = [E(\mathbf{k},\omega) + H_c(\mathbf{k},\omega)]/2, \qquad (16)$$
$$E^-(\mathbf{k},\omega) = [E(\mathbf{k},\omega) - H_c(\mathbf{k},\omega)]/2. \qquad (17)$$

Therefore, computation of the wavenumber-frequency spectra of the energy and of the cross-helicity allows

unique determination of the wavenumber-frequency spectra of the Elsässer fields, and vice-versa.

C. Numerical simulations

To solve numerically the incompressible MHD equations we employ a standard pseudo-spectral code[29,30]. We consider a spatial resolution of $N^3 = 512^3$ grid points, with a second-order Runge-Kutta time integration scheme. Spatial resolution is moderate as we need to store a large amount of data in space and time to compute the correlation functions and spectra defined in Sec. II B. Values considered for the external magnetic field are $B_0 = 0, 0.25$, 1, 2, 4 and 8 (in units of the initial r.m.s. magnetic fluctuations value). We assume periodic boundary conditions in a cube of side $2\pi L$ (with L the initial correlation length of the fluctuations, defined as the unit length). Aliasing is removed by the two-thirds rule truncation method.

The initial condition in all simulations consists of nonzero amplitudes for the $\mathbf{v}(\mathbf{k})$ and $\mathbf{b}(\mathbf{k})$ fields, equipartitioned in all the wavenumbers within shells $1.1 \leq k \leq 4$ (in units of $2\pi L/\lambda$, with λ the wavelength). Random phases are chosen for all Fourier modes in both fields. To keep the system in a turbulent steady state we apply a driving consisting of forcing terms for $\mathbf{b}$ and $\mathbf{v}$, added to Eqs. (1) and (2) in a fixed set of Fourier modes in the band $0.9 \leq k \leq 1.8$. The driving has a random and a time-coherent component, and the correlation time of the forcing is $\tau_f \approx 1$ (of the order of the unit time t_0). To change the level of cross-helicity in the flow, correlations were introduced between the mechanical and electromotive drivings, resulting at late times (depending on the level of cross-correlation between the drivers) in a cross-helicity of $H_c = 0$, 0.3, or 0.9 (these values correspond to the time average in the turbulent steady state; in practice, in each simulation the instantaneous cross-helicity fluctuates in time around the reported mean values).

Note the different values of B_0 and of H_c explored result in a total of 18 simulations. All simulations were continued until the system reached a turbulent steady state, and then continued further to perform the spatio-temporal analysis on the evolution of the Elsässer fields presented in the next section. We will first characterize the spatial behavior of the flows (specially considering the degree of anisotropy as the intensity of the background flow is increased), to then study the behavior of the waves using the spatio-temporal information.

III. RESULTS

A. Wavenumber spectra

After the system reached the turbulent steady state, we analyzed the results during 10 large-scale unit times, after verifying that this time span was enough to ensure convergence of spatio-temporal spectra and correlation functions.

We start discussing the spatial spectral, to characterize the turbulence and to quantify its anisotropy as the intensity of the guide field is varied, for different values of the cross-helicity. The reduced perpendicular energy spectra $E(k_\perp)$ are shown in Fig. 1 for the simulations with $B_0 = 0$, 0.25, 1, 2, 4, and 8 with cross-helicity $H_c = 0.3$. The simulations with $H_c = 0$ and $H_c = 0.9$ have the same behavior. A Kolmogorov power law is also indicated in the figure as reference. As can be seen, despite the moderate spatial resolution of the runs, the observed spatial spectra are compatible with Kolmogorov scaling $\sim k_\perp^{-5/3}$, and the simulations are well resolved displaying a dissipative range for large wavenumbers.

A more detailed behavior of the spectra (and of its anisotropy) can be seen in Fig. 2. There, we show isocontours of the axisymmetric energy spectrum $e(k_\perp, k_\parallel)$ (i.e., the energy density as a function of perpendicular and parallel wavenumbers) for $B_0 = 0$, 1, 4, and 8, and in all cases for flows with $H_c = 0.3$. As a reference we also indicate the curves (in Fourier space) where the Alfvén time is equal to either the sweeping time, or the nonlinear time. In other words, these curves separate regions in which (for theoretical reasons) the fastest time scale can be expected to be either τ_A (above the dashed red curve) or τ_{nl} (below the solid blue curve). The sweeping time can be relevant for all modes below the dashed red curve.

Note that for $B_0 \neq 0$ the energy is not distributed isotropically in the axisymmetric spectra in Fig. 2. Energy tends to accumulate in modes with small $k_\parallel$ as B_0 is increased, and for $B_0 = 4$ and 8, a substantial fraction of the energy accumulates in the vicinity of the curves satisfying $\tau_A \approx \tau_{sw}$ and $\tau_A \approx \tau_{nl}$.

B. Wavenumber-frequency spectra

The main results of the present study are summarized in Figs. 3 to 6, which quantify the spatio-temporal behavior of the Elsässer fields separately. These figures show the normalized wavevector and frequency spectra of the $\mathbf{z}^+$ and $\mathbf{z}^-$ variables, for simulations with different values of the background mean field B_0 and cross-helicity H_c. As the spectra are multidimensional, in all cases we show slices of the spectrum for $k_\perp = 0$ and as a function of $k_\parallel$ and ω.

Figure 3 shows these spatio-temporal spectra for simulations with $B_0 = 0$. In this case, the dispersion relation for Alfvénic fluctuations becomes $\omega = 0$, and Alfvén waves are indistinguishable (in this spectrum) from slow modes such as turbulent eddies. The sweeping relation, for eddies with velocity v_{rms}, becomes $\omega = \pm v_{rms} k_\parallel$, and in practice, as all turbulent eddies with this velocity (or a smaller velocity) can sweep randomly small-scale structures in the flow, the relation for random sweeping becomes $|\omega| \leq v_{rms} k_\parallel$. Both relations are indicated re-

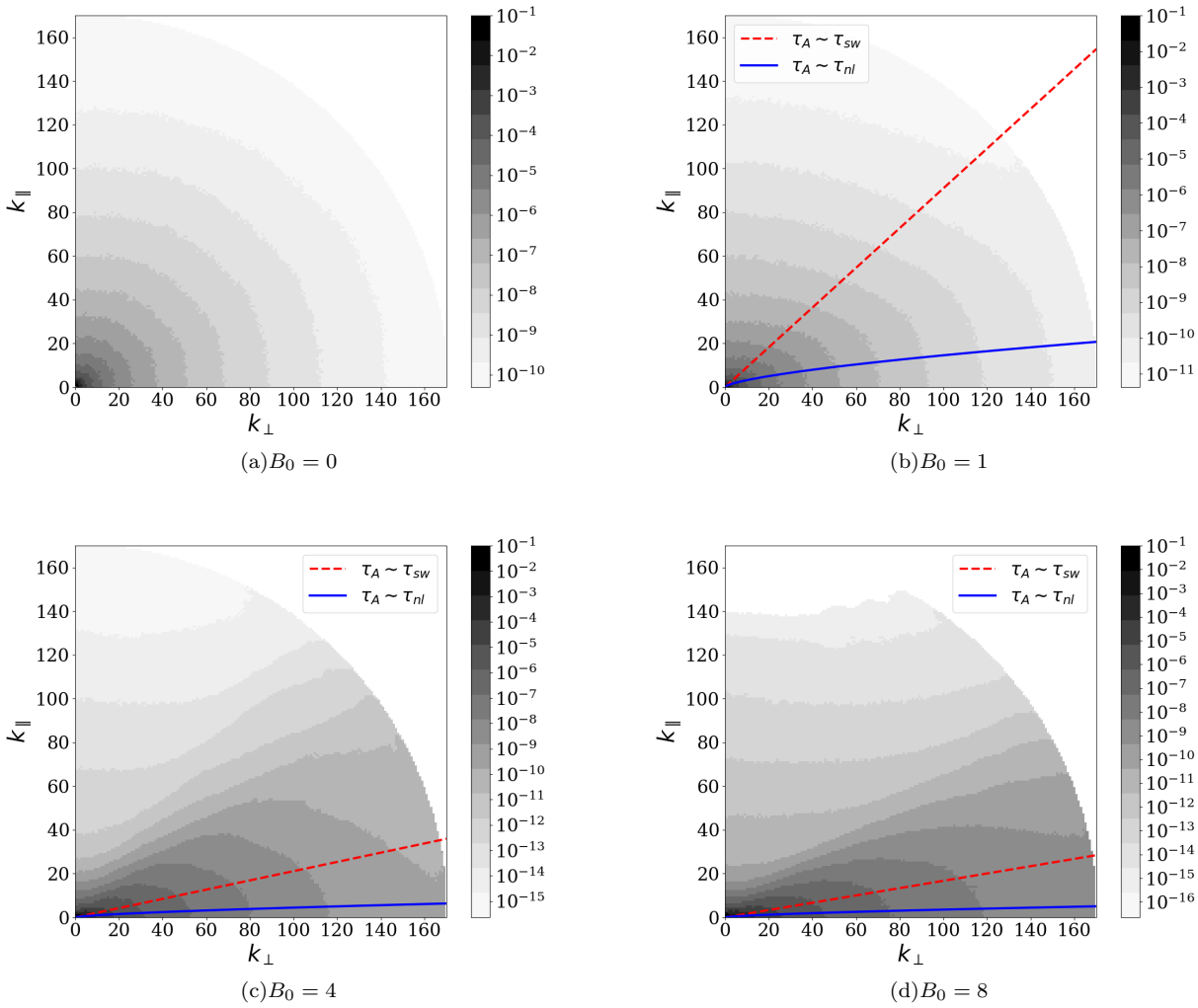

(a)$B_0 = 0$ (b)$B_0 = 1$

(c)$B_0 = 4$ (d)$B_0 = 8$

FIG. 2. Isocontours of the axisymmetric energy spectrum $e(k_\perp, k_\parallel)$ for $B_0 = 0$, 1, 4 and 8, and for $H_c = 0.3$. In all cases, dark means larger energy density (in logarithmic scale). The lines indicate the modes for which the sweeping time (red dashed line) or the local non-linear time (solid blue line) become equal to the Alfvén time. For large B_0 the flow becomes more anisotropic, and isocontours change shape as they cross these lines. Note also the increase in the energy in modes that have the Alfvén time as the fastest time (i.e., of modes below the solid blue curve) as B_0 increases.

spectively by dashed and solid lines in Fig. 3.

Accumulation of energy in the spectra in Fig. 3 can be seen for all modes in the region enclosed by the the sweeping relation, evidencing the presence of broadband (strong) turbulence rather than wave turbulence or linear wave propagation. Nevertheless, for large values of the cross-helicity ($H_c = 0.9$), energy accumulates instead in modes with $\omega \approx 0$, and more energy can be observed in $\mathbf{z}^+$ fluctuations when compared to the $\mathbf{z}^-$ fluctuations. From these spectra we can conclude that for $B_0 = 0$ and $H_c = 0$ the dominant timescale is that of the sweeping, while for large values of $H_c = 0$ either the non-linear timescale or the Alfvén time become dominant.

Figure 4 shows the spatio-temporal spectra for simulations with $B_0 = 0.25$. The case with $H_c = 0$ shows again a broad range of fluctuations in the range of frequencies enclosed by the sweeping relation. As the value of H_c is increased the $\mathbf{z}^+$ fluctuations become dominant, a situation which is more evident in the case with $H_c = 0.9$. Also, as H_c is increased, energy in $\mathbf{z}^+$ fluctuations leaves the funnel defined by the sweeping relation, and concentrates in the vicinity of the dispersion relation of Alfvén waves $\omega^+ = +\mathbf{V}_\mathrm{A} \cdot \mathbf{k}$ (see the case with $H_c = 0.9$ in Fig. 4). Note that for waves described by $\mathbf{z}^\pm = \mathbf{z}_0^\pm e^{i(\mathbf{k}\cdot\mathbf{x}+\omega^\pm t)}$ (where the choice of signs follows from the fact that the Fourier transforms used in space and in time follow the same sign convention, and where $\mathbf{z}_0^\pm$ are the amplitudes of the waves), the sign of ω^+ implies $\mathbf{z}^+$ fluctuations propagate anti-parallel to the guide field, as expected. However, in an apparent contradiction, the waves with the opposite polarization, i.e., the $\mathbf{z}^-$ fluctuations, also populate (albeit with smaller

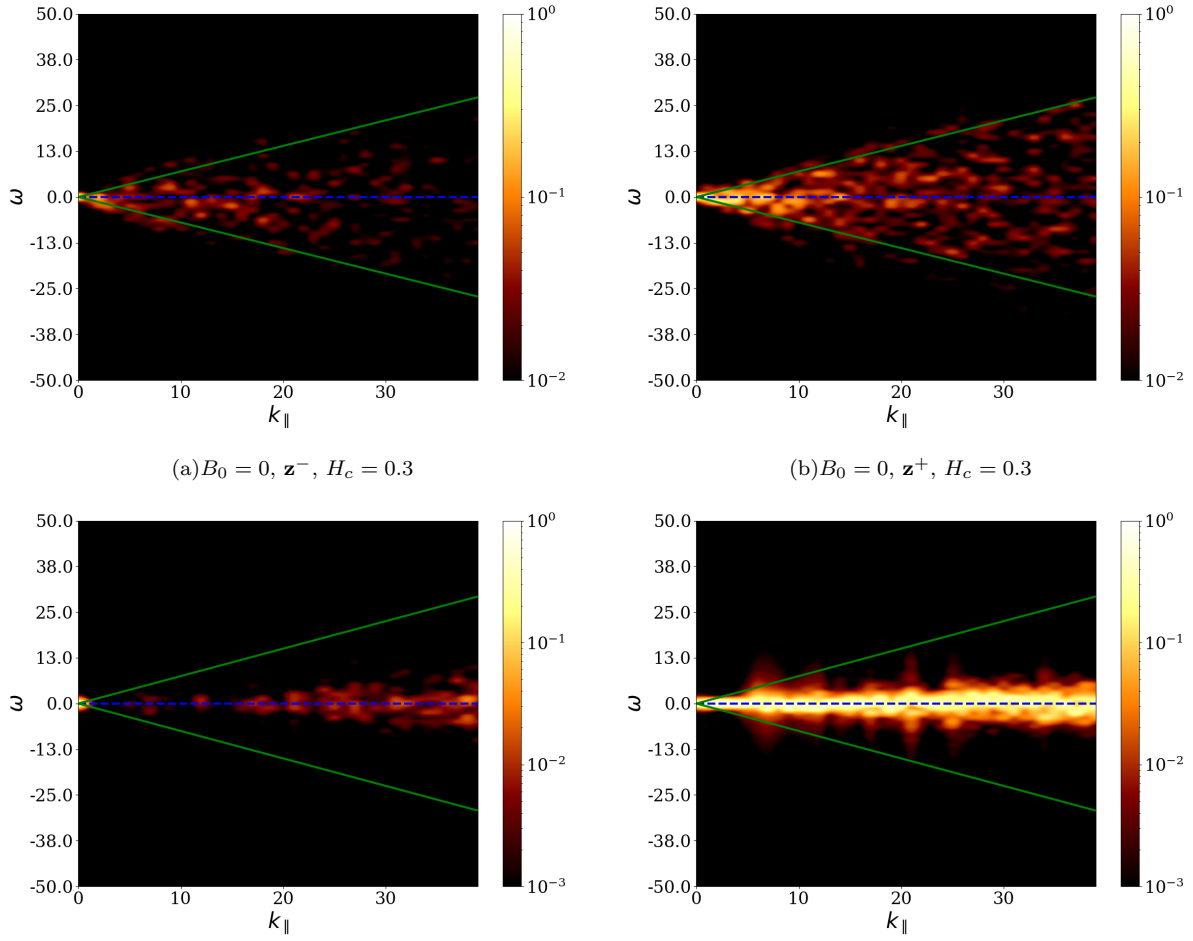

(a)$B_0 = 0$, $\mathbf{z}^-$, $H_c = 0.3$

(b)$B_0 = 0$, $\mathbf{z}^+$, $H_c = 0.3$

(c)$B_0 = 0$, $\mathbf{z}^-$, $H_c = 0.9$

(d)$B_0 = 0$, $\mathbf{z}^+$, $H_c = 0.9$

FIG. 3. Normalized wave vector and frequency spectra $E^{\pm}(\mathbf{k},\omega)/E^{+}(\mathbf{k})$ of $\mathbf{z}^-$ (left) and $\mathbf{z}^+$ (right), for the isotr[illegible] simulations ($B_0 = 0$) with $H_c = 0.3$ [top, panels (a) and (b)] and $H_c = 0.9$ [bottom, panels (c) and (d)], as a function of $k_\parallel$ and for fixed $k_\perp = 0$. Lighter regions indicate larger energy density. The spectra correspond to the power in the time and space Fourier transform of the fields, such that accumulation of energy in modes near the dispersion relation (or in all modes below the sweeping curve) points to a dominance of a physical effect (i.e., of its associated frequency) in the dynamics of a given scale $\sim 1/k_\parallel$. As a reference, the sweeping time relation giving by Eq. (12) is indicated by solid (green) lines. A broad excitation of modes is observed for all modes with $\omega \leq 1/\tau_{sw}$ (sweeping) in panels (a) and (b), and for $\omega \approx 0$ in panels (c) and (d).

amplitude) the same upper branch of the Alfvénic wave dispersion relation. As the $\mathbf{z}^-$ fluctuations satisfy another dispersion relation ($\omega^- = -\mathbf{V}_\mathrm{A} \cdot \mathbf{k}$), in the linear regime these fluctuations should populate instead the lower branch of the dispersion relation shown in Fig. 4. This behavior indicates that $\mathbf{z}^-$ fluctuations also propagate in real space in the direction anti-parallel to the guide field (i.e., with negative velocity), instead of parallel to this field (i.e., with positive velocity) as expected.

As B_0 is increased, this effect becomes more evident. In Fig. 5 we show the spatio-temporal spectra for simulations with $B_0 = 1$. Now energy tends to concentrate near the dispersion relation of the Alfvén waves for all values of H_c, i.e., as we increase the value of B_0 the relevance of random sweeping decreases and Alfvén waves become more important. For $H_c = 0$ we observe waves propagating in both directions: $\mathbf{z}^+$ fluctuations propagate anti-parallel to the guide field, and $\mathbf{z}^-$ fluctuations propagate parallel to this field. Also, for values of $k_\parallel$ larger than ≈ 20, the dispersion in the excitation of modes increases and energy starts to populate the funnel in spectral space associated with sweeping, indicating random sweeping plays a role at small vertical scales. Instead, for $H_c = 0.3$ and 0.9 energy accumulates only near the wave dispersion relation, and we recover counter-propagation of one of the wave motions: both $\mathbf{z}^+$ and $\mathbf{z}^-$ fields propagate in the same direction, anti-parallel to the guide field. Increasing B_0 further reduces this effect (see the cases with $B_0 = 8$ in Fig. 6), resulting in the expected propagation for each excitation, or in very little or no propagation of $\mathbf{z}^-$ when H_c is sufficiently small.

What is the origin of the observed $\mathbf{z}^-$ fluctuations

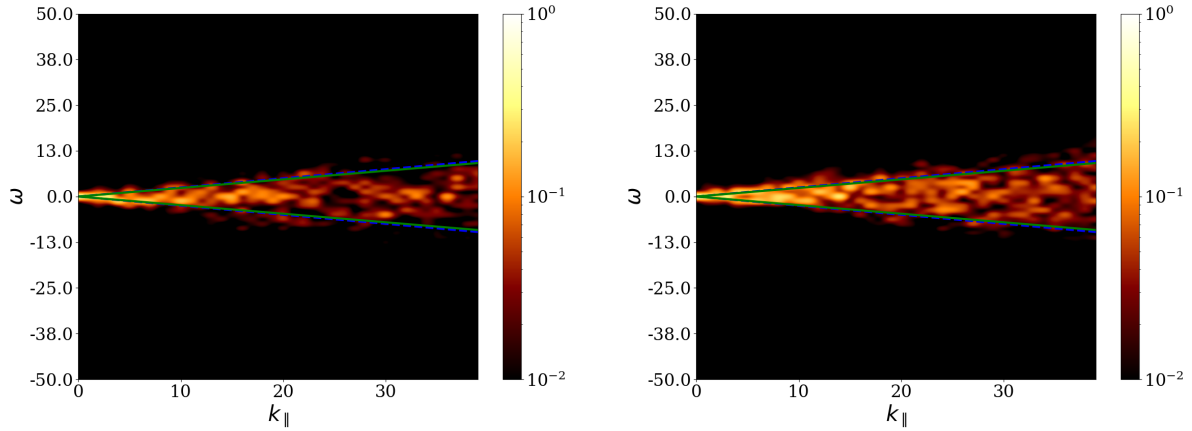

(a)$B_0 = 0.25$, $\mathbf{z}^-$, $H_c = 0$

(b)$B_0 = 0.25$, $\mathbf{z}^+$, $H_c = 0$

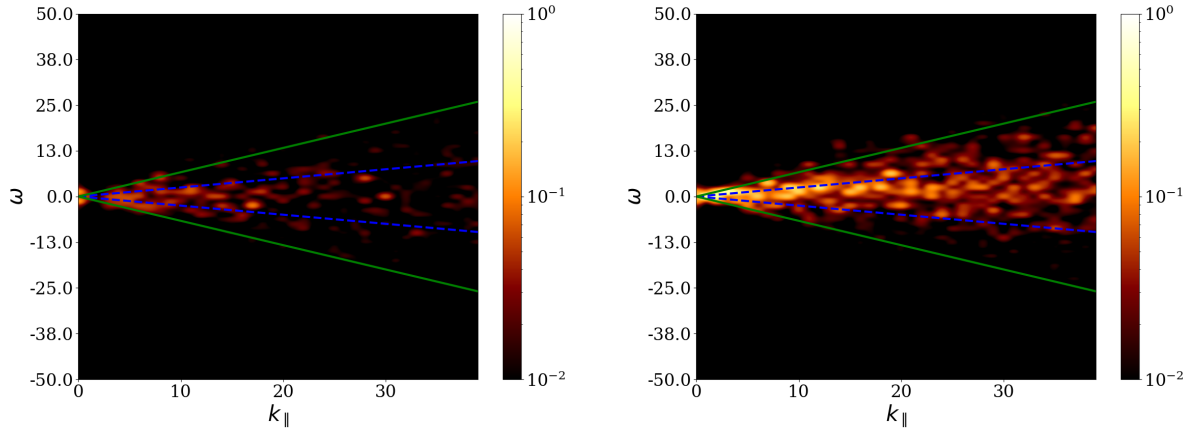

(c)$B_0 = 0.25$, $\mathbf{z}^-$, $H_c = 0.3$

(d)$B_0 = 0.25$, $\mathbf{z}^+$, $H_c = 0.3$

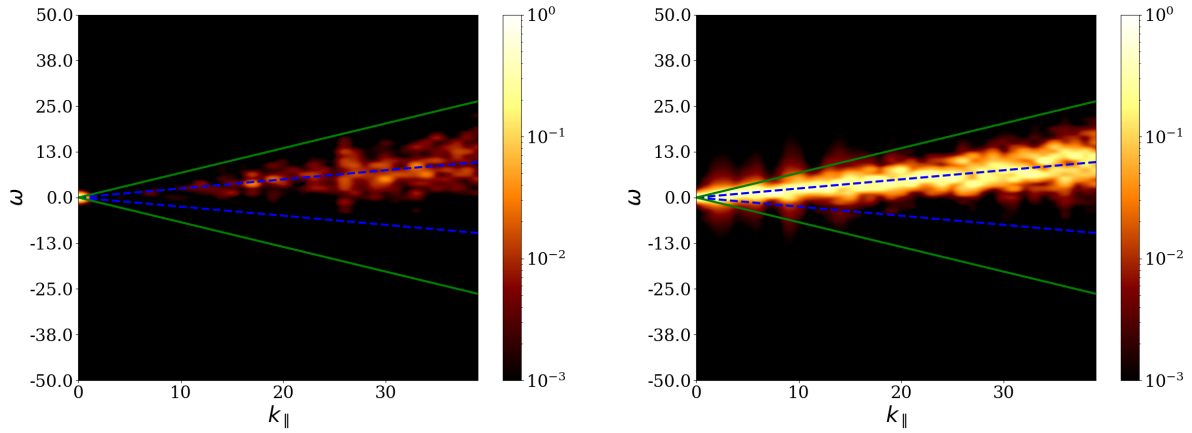

(e)$B_0 = 0.25$, $\mathbf{z}^-$, $H_c = 0.9$

(f)$B_0 = 0.25$, $\mathbf{z}^+$, $H_c = 0.9$

FIG. 4. Normalized spectra $E^{\pm}(\mathbf{k},\omega)/E^{+}(\mathbf{k})$ of $\mathbf{z}^-$ (left) and $\mathbf{z}^+$ (right), for the runs with $B_0 = 0.25$, for modes with $k_\perp = 0$, and thus as a function of $k_\parallel$ and ω. Panels (a) and (b) correspond to $H_c = 0$, (c) and (d) to $H_c = 0.3$, and (e) and (f) to $H_c = 0.9$. Labels are as in Fig. 3, and the dashed (blue) line indicates the dispersion relation of Alfvén waves. For low H_c sweeping is the dominant effect, while for large H_c energy accumulates near the dispersion relation of the waves, albeit for both $\mathbf{z}^+$ and $\mathbf{z}^-$ with the same sign.

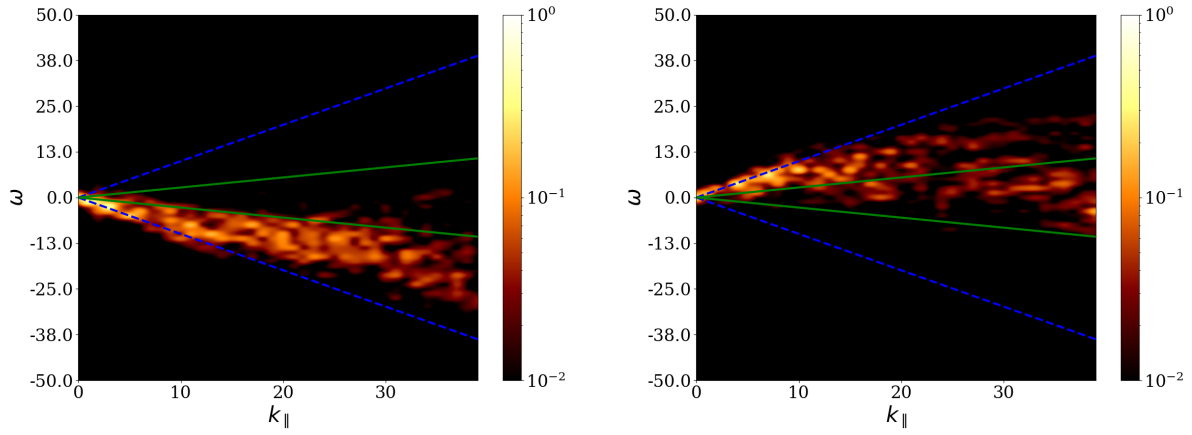

(a)$B_0 = 1.0$, $\mathbf{z}^-$, $H_c = 0$

(b)$B_0 = 1.0$, $\mathbf{z}^+$, $H_c = 0$

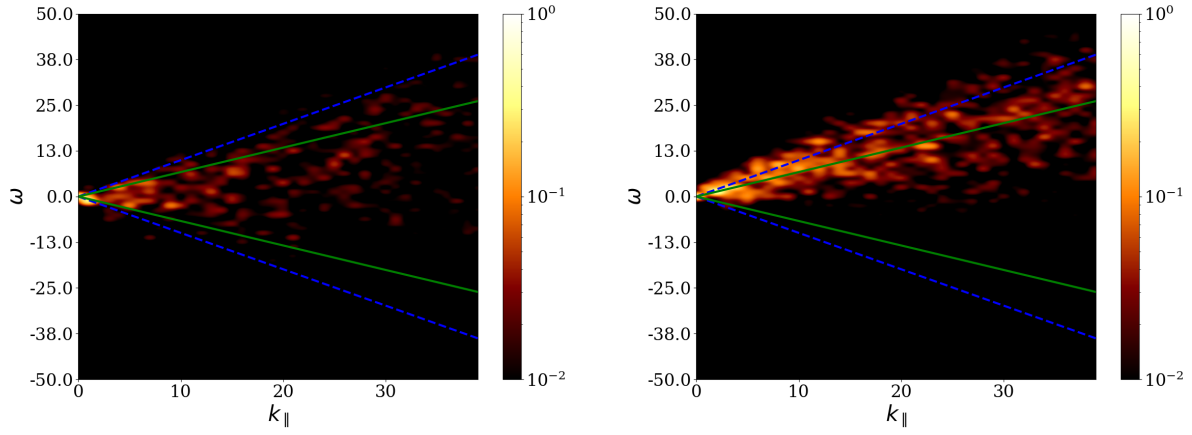

(c)$B_0 = 1.0$, $\mathbf{z}^-$, $H_c = 0.3$

(d)$B_0 = 1.0$, $\mathbf{z}^+$, $H_c = 0.3$

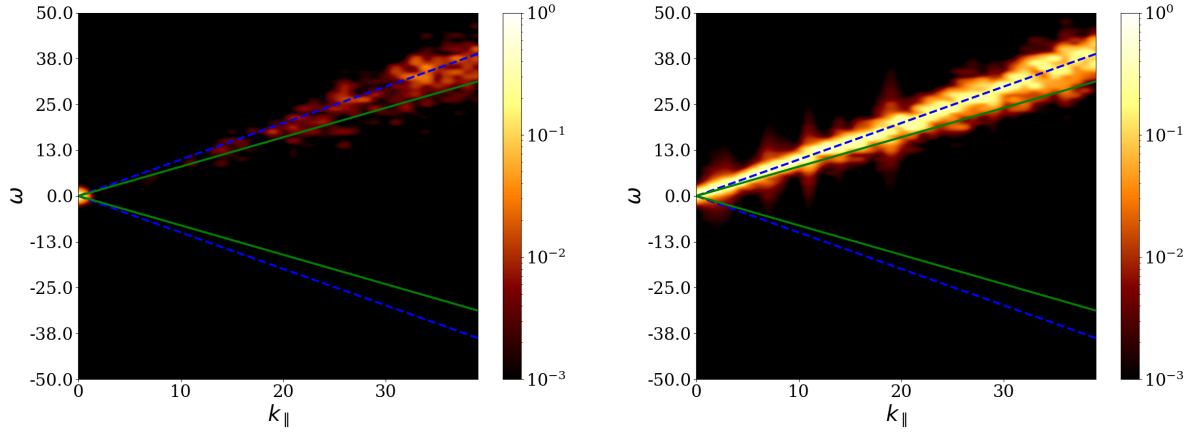

(e)$B_0 = 1.0$, $\mathbf{z}^-$, $H_c = 0.9$

(f)$B_0 = 1.0$, $\mathbf{z}^+$, $H_c = 0.9$

FIG. 5. Same as in Fig. 4, for the runs with $B_0 = 1$. Panels (a) and (b) correspond to $H_c = 0$, (c) and (d) to $H_c = 0.3$, and (e) and (f) to $H_c = 0.9$. Labels are as in Fig. 3. In this case power for $H_c = 0$ is concentrated in a region near the wave dispersion relations $\omega^{\pm} \approx \pm \mathbf{V}_\mathrm{A} \cdot \mathbf{k}$ up to $k_\parallel \approx 10$. For $H_c = 0.9$, both fields $\mathbf{z}^+$ and $\mathbf{z}^-$ follow the same dispersion relation $\omega \approx +\mathbf{V}_\mathrm{A} \cdot \mathbf{k}$ and Alfvénic excitations dominate over all scales.

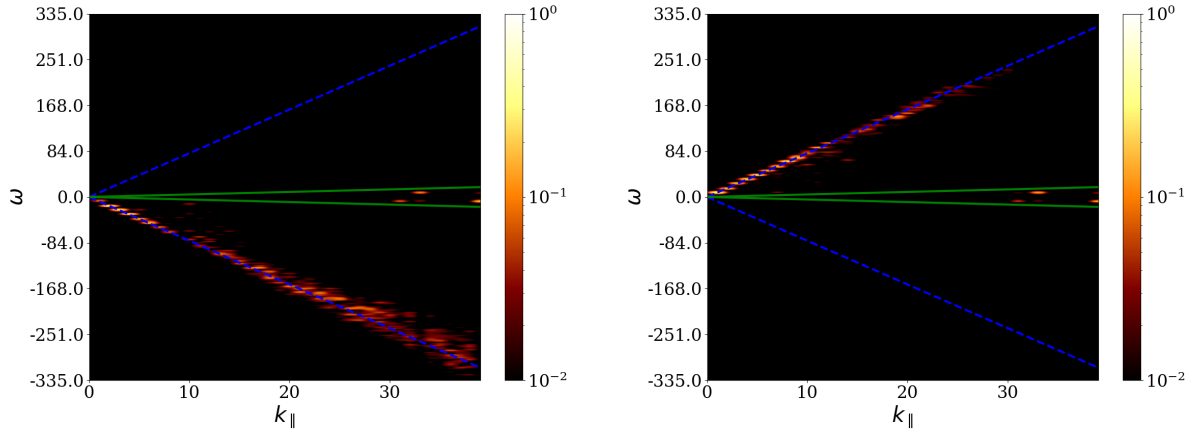

(a)$B_0 = 8.0$, $\mathbf{z}^-$, $H_c = 0$

(b)$B_0 = 8.0$, $\mathbf{z}^+$, $H_c = 0$

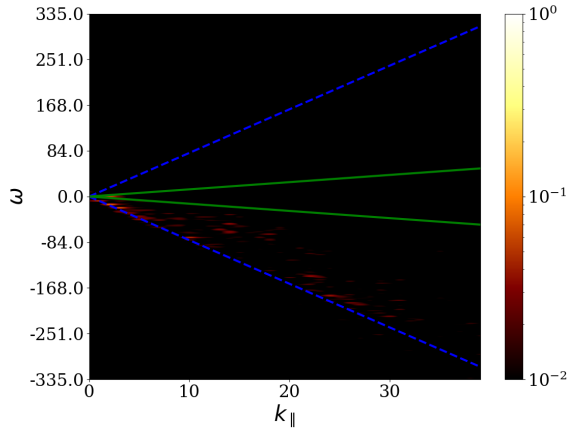

(c)$B_0 = 8.0$, $\mathbf{z}^-$, $H_c = 0.3$

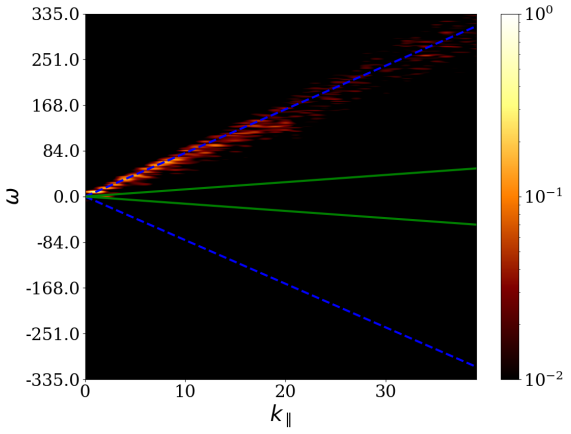

(d)$B_0 = 8.0$, $\mathbf{z}^+$, $H_c = 0.3$

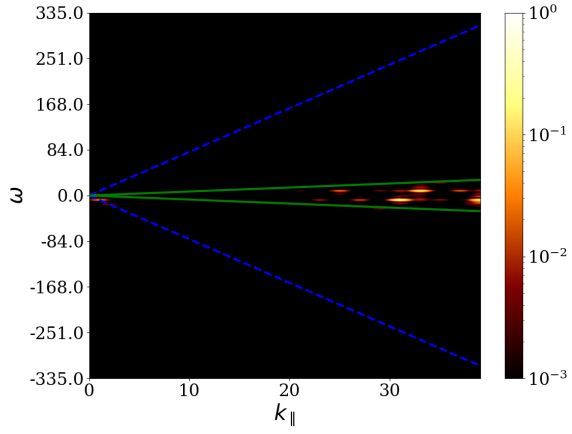

(e)$B_0 = 8.0$, $\mathbf{z}^-$, $H_c = 0.9$

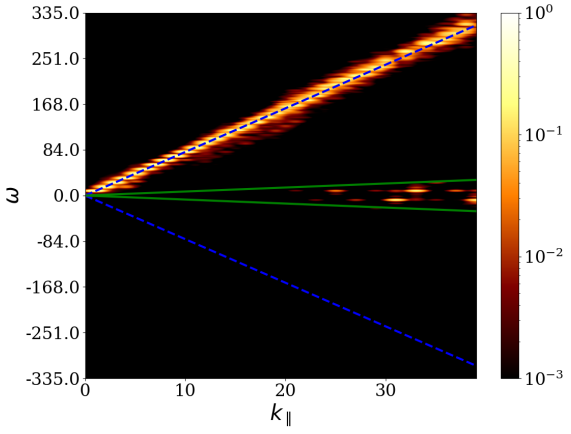

(f)$B_0 = 8.0$, $\mathbf{z}^+$, $H_c = 0.9$

FIG. 6. Same as in Fig. 4, for the runs with $B_0 = 8$. In all cases power is concentrated in a narrow region near the wave dispersion relations $\omega^\pm \approx \pm \mathbf{V}_\mathrm{A} \cdot \mathbf{k}$ or near $\omega \approx 0$, for all the wavenumbers studied, and there is no evidence of counter-propagation.

propagating in the same direction as the $\mathbf{z}^+$ fluctuations? From Eq. (7), they must be caused by reflections in large scale inhomogeneities of the mean magnetic field (note there is no mean background flow in our simulations). Although our background guide field B_0 is uniform (i.e., constant in space as well as in time), the total mean field a fluctuation sees includes a slowly varying component (e.g., from magnetic field fluctuations at large scales, such

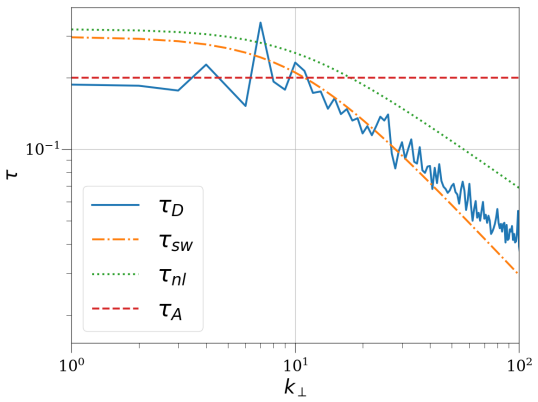

(a)$\mathbf{z}^-$, $B_0 = 1$, $H_c = 0.3$, $k_\parallel = 10$

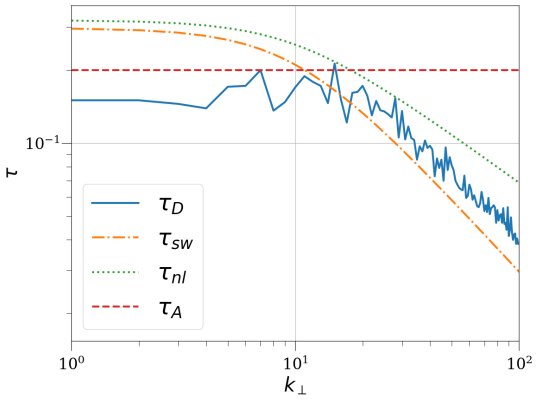

(b)$\mathbf{z}^+$, $B_0 = 1$, $H_c = 0.3$, $k_\parallel = 10$

FIG. 7. Decorrelation times τ_D for the run with $B_0 = 1$ and $H_c = 0.3$, for $k_\parallel = 10$ constant and as a function of $k_\perp$. Panel (a) corresponds to $\mathbf{z}^-$ and panel (b) to $\mathbf{z}^+$. The theoretical prediction for the sweeping time τ_{sw}, the non-linear time τ_{nl}, and the Alfvén time τ_A are indicated as references.

as those in $k = 1$ modes, which evolve on a slower time scale than fast waves and small-scale fluctuations). As a result, the flow has an effective Alfvén velocity that depends on the spatial coordinates. We can then write for either type of Elsässer fluctuations the ideal linearized Eq. (7) for constant density and for $\mathbf{U} = 0$ (no mean background flow) as

$$\partial_t \mathbf{z}^\pm = \pm \mathbf{V}_\mathrm{A} \cdot \nabla \mathbf{z}^\pm \mp \mathbf{z}^\mp \cdot \frac{\nabla \mathbf{B}'}{\sqrt{4\pi\rho}}, \tag{18}$$

where $\mathbf{V}_\mathrm{A}$ can now include large-scale fluctuations of the magnetic field, and $\mathbf{B}'$ as before is the total magnetic field in Gaussian units. If the cross-helicity H_c is close to 1, that is, if $|\mathbf{z}^+| \gg |\mathbf{z}^-|$, we have for $\mathbf{z}^+$

$$\partial_t \mathbf{z}^+ \approx \mathbf{V}_\mathrm{A} \cdot \nabla \mathbf{z}^+, \tag{19}$$

and using $\mathbf{z}^\pm = \mathbf{z}_0^\pm e^{i(\mathbf{k}\cdot\mathbf{x} + \omega^\pm t)}$ we recover the usual dispersion relation for waves propagating anti-parallel to the mean field $\omega^+ = +\mathbf{V}_\mathrm{A} \cdot \mathbf{k}$ (where now $\mathbf{V}_\mathrm{A}$ can fluctuate slowly in space and time). However, for $\mathbf{z}^-$ we obtain

$$\partial_t \mathbf{z}^- \approx -\mathbf{V}_\mathrm{A} \cdot \nabla \mathbf{z}^- + \mathbf{z}^+ \cdot \frac{\nabla \mathbf{B}'}{\sqrt{4\pi\rho}}. \tag{20}$$

This equation indicates that the propagation of $\mathbf{z}^-$ perturbations (which are smaller in amplitude than $\mathbf{z}^+$) can be strongly affected by the $\mathbf{z}^+$ field and by spatial variations of the large-scale magnetic field.

From Eq. (20) we can also extract some phenomenological conditions for the behavior seen in Figs. 3 to 6 (and in particular, for the counter-propagation of waves) to take place. Using again $\mathbf{z}^\pm = \mathbf{z}_0^\pm e^{i(\mathbf{k}\cdot\mathbf{x} + \omega^\pm t)}$, and assuming $\mathbf{B}' = \mathbf{B}'_0 + \mathbf{b}'_0$ where $\mathbf{b}'_0 = \tilde{\mathbf{b}}'_0 e^{i\mathbf{K}\cdot\mathbf{x}}$ is the slowly varying large-scale magnetic field with wavenumber $K \ll k$, Eq. (20) reduces to

$$\left(\omega^- + \mathbf{V}_\mathrm{A} \cdot \mathbf{k}\right) \mathbf{z}_0^- e^{i\omega^- t} = \frac{\left(\mathbf{K} \cdot \mathbf{z}_0^+\right) \mathbf{b}'_0}{\sqrt{4\pi\rho}} e^{i\omega^+ t}. \tag{21}$$

Taking the dot product with $\mathbf{z}_0^-$, defining Elsässer energy densities $e^\pm = |\mathbf{z}_0^\pm|^2/4$, and defining the fluctuations in the Alfvén velocity (associated to the large-scale magnetic field fluctuations) as $\mathbf{v}_\mathrm{A} = \mathbf{b}'_0/\sqrt{4\pi\rho}$, we finally get

$$\left(\omega^- + \mathbf{V}_\mathrm{A} \cdot \mathbf{k}\right) e^{i\omega^- t} = \frac{\left(\mathbf{K} \cdot \mathbf{z}_0^+\right) \left(\mathbf{v}_\mathrm{A} \cdot \mathbf{z}_0^-\right)}{4e^-} e^{i\omega^+ t}. \tag{22}$$

This equation admits solutions

$$\omega^- = \omega^+ = +\mathbf{V}_\mathrm{A} \cdot \mathbf{k}, \tag{23}$$

$$2\mathbf{V}_\mathrm{A} \cdot \mathbf{k} = \left(\mathbf{K} \cdot \mathbf{z}_0^+\right) \left(\mathbf{v}_\mathrm{A} \cdot \mathbf{z}_0^-\right) / (4e^-), \tag{24}$$

which correspond to both waves traveling in the same direction as long as the second condition, given by Eq. (24), can be fulfilled. From dimensional analysis, this condition requires that

$$2\frac{V_\mathrm{A}}{v_\mathrm{A}} \frac{k}{K} \sim \sqrt{\frac{e^+}{e^-}}, \tag{25}$$

which (as $V_\mathrm{A} \gtrsim v_\mathrm{A}$ and $k \gg K$) cannot be satisfied when $H_c \approx 0$ (as observed in Figs. 3 to 6), or when the guide field becomes too strong for a fixed value of H_c (as also observed in the spatio-temporal spectra). Thus, this last qualitative argument indicates (in agreement with the simulations) that $\mathbf{z}^-$ fluctuations can propagate with the same phase speed and direction as the $\mathbf{z}^+$ fluctuations as long as $H_c \neq 0$ and B_0 is not too strong for a fixed value of the cross-helicity.

In other words, if $|\mathbf{z}^+|$ at large scales is comparable to $|\mathbf{V}_\mathrm{A}|$ and $H_c \approx 1$, we can see $\mathbf{z}^-$ fluctuations propagate in the same direction as $\mathbf{z}^+$ fluctuations as the result of reflections in inhomogeneities of the large-scale magnetic field (a similar behavior can result from mass density fluctuations when the flow is compressible, as is the case in some regions of the solar wind and the interplanetary medium, and this argument does not preclude other effects such as strong non-linear interactions from also

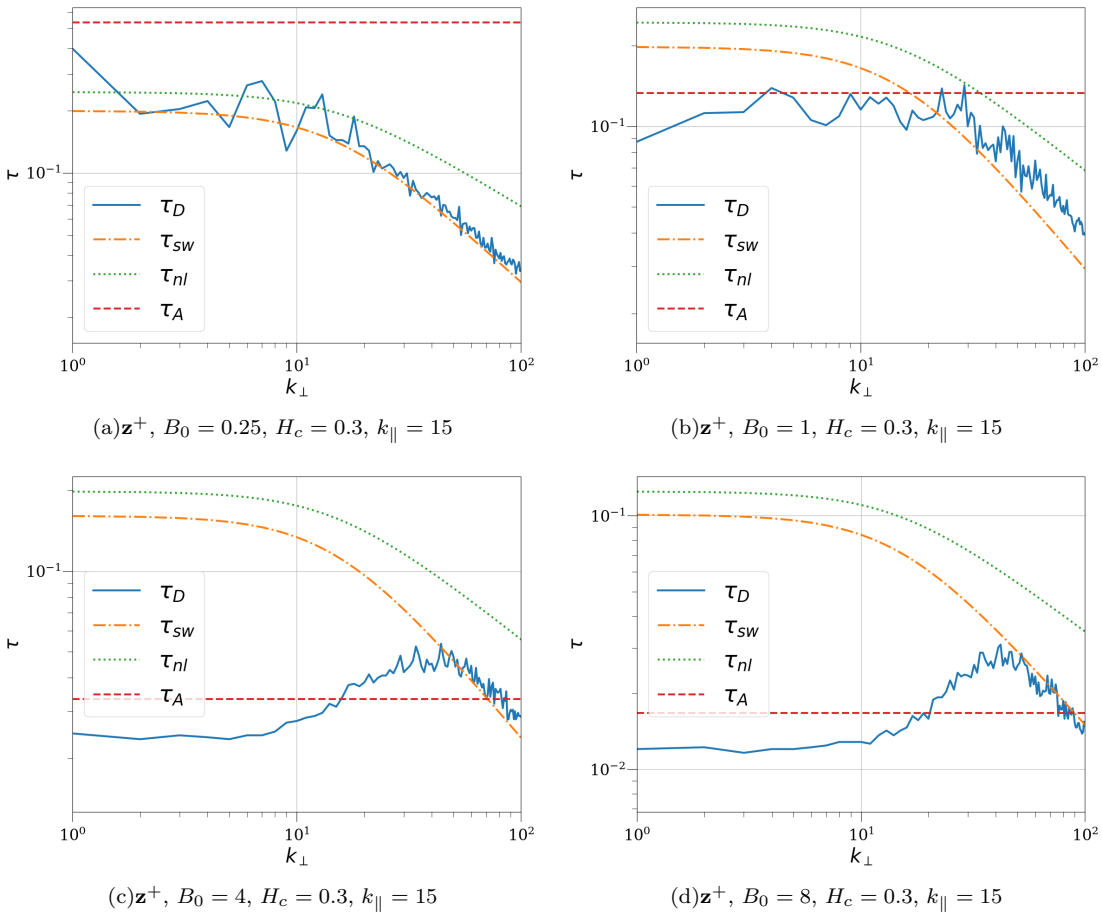

(a)$\mathbf{z}^+$, $B_0 = 0.25$, $H_c = 0.3$, $k_\parallel = 15$

(b)$\mathbf{z}^+$, $B_0 = 1$, $H_c = 0.3$, $k_\parallel = 15$

(c)$\mathbf{z}^+$, $B_0 = 4$, $H_c = 0.3$, $k_\parallel = 15$

(d)$\mathbf{z}^+$, $B_0 = 8$, $H_c = 0.3$, $k_\parallel = 15$

FIG. 8. Decorrelation times τ_D for the $\mathbf{z}^+$ field in simulations with $H_c = 0.3$ and (a) $B_0 = 0.25$, (b) 1, (c) 4, and (d) 8, for $k_\parallel = 15$ and as a function of $k_\perp$. As in Fig. 7, several curves with theoretical predictions for the decorrelation times are shown as references.

resulting in reflection and counter-propagation of excitations). Moreover, when the intensity of the background magnetic field $\mathbf{B}_0$ is further increased, the arguments used above are not valid anymore and the relevance of the reflections reduces. This is compatible with the behavior seen in Fig. 6 for the simulations with $B_0 = 8$, which show similar amounts of power in both type of fluctuations when $H_c = 0$, less power in $\mathbf{z}^-$ fluctuations when $H_c = 0.3$ (and propagating opposite to the $\mathbf{z}^+$ field), and no appreciable power for $\mathbf{z}^-$ fluctuations when compared to $\mathbf{z}^+$ in the case with $H_c = 0.9$.

C. Decorrelation times

From the discussions in Sec. II B, another way to identify dominant time scales for individual modes is to study the decorrelation time τ_D, i.e., the time it takes for each Fourier mode with wave vector $\mathbf{k}$ to be decorrelated from its previous history either by non-linear eddy interactions (if $\tau_D \sim \tau_{nl}$), by the cross-over of waves (if $\tau_D \sim \tau_A$), or by the sweeping by the large-scale flow (when $\tau_D \sim \tau_{sw}$). Again, as τ_D depends on the wave vector $\mathbf{k}$, in the following we show it for fixed values of $k_\parallel$ or $k_\perp$, and as a function of the remaining wavenumber. In all cases, the decorrelation time τ_D is obtained from the numerical data by computing the correlation function $\Gamma(k_\perp, k_\parallel, \tau)$, and looking at the value of the time lag τ for which the correlation function decays to $1/e$ from its value for $\tau = 0$, that is, the characteristic time for the decay of the correlation function[17].

Figure 7 shows the different decorrelation times for a fixed value of $k_\parallel = 10$ and as a function of $k_\perp$, for the simulation with $B_0 = 1$ and $H_c = 0.3$. The theoretical predictions for the different decorrelation times are also indicated as a reference. Since the Alfvénic time is independent of $k_\perp$ it shows as a constant vale in this figure. The decorrelation time τ_D obtained from the numerical data is very close to the Alfvénic time for small values of $k_\perp$ (up to $k_\perp \approx 10$), but it deviates and becomes closer to the sweeping time for large values of $k_\perp$ (i.e, for small perpendicular lengthscales). This is more clear for $\mathbf{z}^-$ fluctuations than for $\mathbf{z}^+$ fluctuations, for which the decorrelation time τ_D for $k_\perp > 10$ is in between the

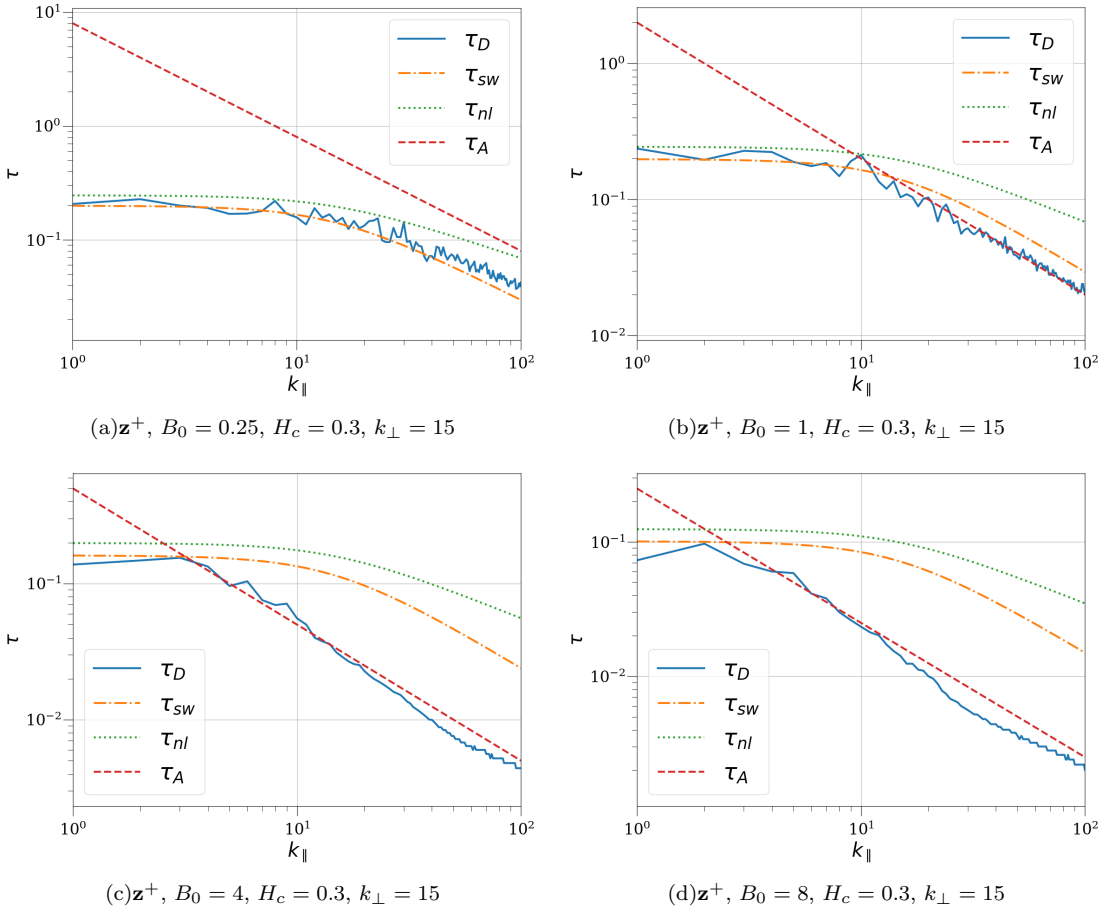

(a)$\mathbf{z}^+$, $B_0 = 0.25$, $H_c = 0.3$, $k_\perp = 15$

(b)$\mathbf{z}^+$, $B_0 = 1$, $H_c = 0.3$, $k_\perp = 15$

(c)$\mathbf{z}^+$, $B_0 = 4$, $H_c = 0.3$, $k_\perp = 15$

(d)$\mathbf{z}^+$, $B_0 = 8$, $H_c = 0.3$, $k_\perp = 15$

FIG. 9. Same as in Fig. 8 for $k_\perp = 15$ fixed, and as a function of $k_\parallel$.

scaling of τ_{sw} and of τ_{nl}.

Figure 8 shows the decorrelation times τ_D for the $\mathbf{z}^+$ field for cases with $H_c = 0.3$, with a guide field of $B_0 = 0.25$, 1, 4, and 8, and for fixed $k_\parallel = 15$ as a function of $k_\perp$. Again, for low values of B_0, τ_D is mostly dominated for the sweeping, either for all values of $k_\perp$ (for $B_0 = 0.25$) or down to $k_\perp \approx 20$ (for $B_0 = 1$). However, for larger values of B_0 (or for small values of $k_\perp$ when $B_0 = 1$) Alfvénic effects become dominant, with τ_D taking values close to τ_A. Overall, the fastest time scale at any given $k_\perp$ seems to be the dominant one. These results are consistent with the previous ones we obtained[17] for the case of strong incompressible MHD turbulence with no cross-helicity, although the presence of some cross-helicity in the flow seems to favor a transition towards a flow more dominated by Alfvén waves as also seen in the spatio-temporal spectra in Sec. III B.

This behavior can also be seen when $k_\perp$ is fixed, and τ_D is studied as a function of $k_\parallel$ (see Fig. 9). For simulations with $H_c = 0.3$ and with increasing B_0, we see that τ_D varies with $k_\parallel$ as τ_{sw} when B_0 is small or moderate and when $k_\parallel$ is small, and varies as τ_A when B_0 or $k_\parallel$ are sufficiently large. In other words, modes with wave vectors sufficiently aligned with the guide field are dominated by the Alfvén time. And again, the fastest time scale in this figure is the one that dominates the dynamics.

However, and as mentioned before, this picture changes when H_c is sufficiently large. This can be seen in Fig. 10, where the decorrelation time τ_D is plotted for the simulations with $B_0 = 1$, for fixed $k_\perp = 40$, and as a functions of $k_\parallel$ for $H_c = 0$, 0.3 and 0.9. While for small values of H_c we observe the same behavior as before, for large values of H_c the Alfvén time becomes dominant, even when it is slower than all the other time scales, as in the case of the simulation with $H_c = 0.9$ and small values of $k_\parallel$.

Thus, while for small values of H_c the analysis of the decorrelation time confirms the tendency observed in our previous study[17] that the sweeping time dominates the decorrelations except for the cases with medium and large values of B_0 where the Alfvénic time is dominant for small values of $k_\perp$ or large values of $k_\parallel$ (see also studies of MHD turbulence in the weak regime, or of the transition from weak to strong MHD turbulence in Refs.[16–18]), increasing the cross-helicity content of the flow has interesting consequences. The appearance of the Alfvénic time as dominant becomes more clear for large values of H_c, even when it is not the fastest time scale, and consis-

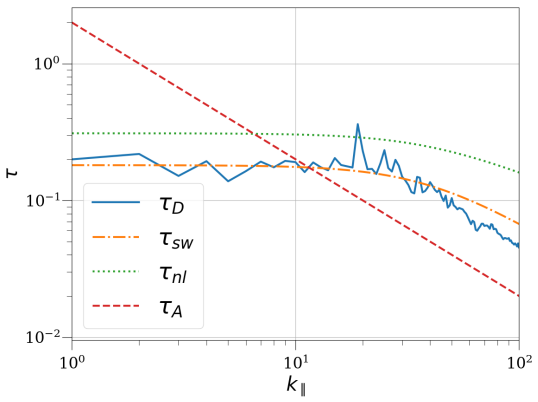

(a)$H_c = 0$

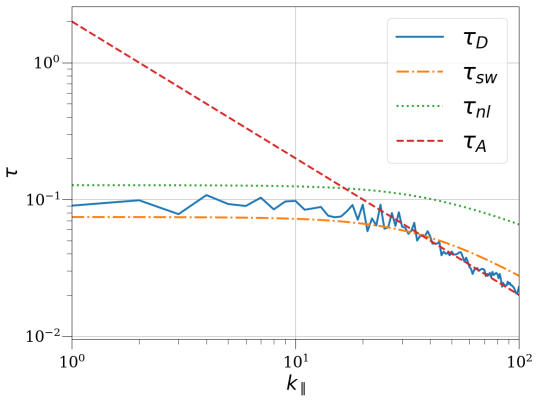

(b)$H_c = 0.3$

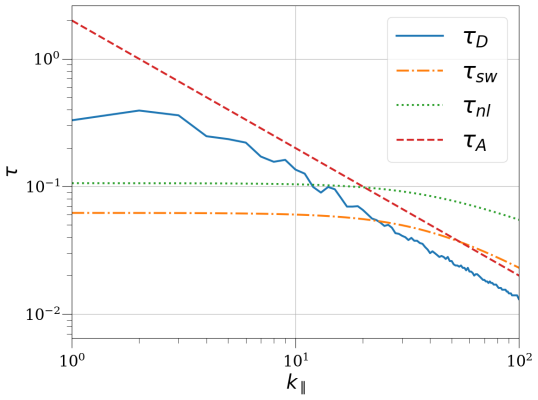

(c)$H_c = 0.9$

FIG. 10. Decorrelation times τ_D for the runs with $B_0 = 1$, for $k_\perp = 40$ and as a function of $k_\parallel$. The panels correspond to (a) $H_c = 0$, (b) 0.3, and (c) $H_c = 0.9$. References are as in Fig. 8.

tent with a linear (or weakly non-linear) picture in which most of the fluctuations have a single direction of propagation. However, as evidenced in the spatio-temporal analysis of the energy spectrum of each Elsässer field as a function of $\mathbf{k}$ and ω, inhomengeneities of the large scale magnetic field can induce reflections, and turn on non-linear interactions dominated by the Alfvén cross-over time between waves for modes with wave vectors sufficiently aligned with the guide field, or by the sweeping or non-linear time for other modes.

IV. CONCLUSIONS

We analyzed the spatio-temporal behavior of MHD fluctuations considering their polarizations in terms of the Elsässer variables, using direct numerical simulations of three-dimensional incompressible MHD turbulence. We considered cases with relatively small, intermediate, and large values of a mean background magnetic field, and with null, small, and high cross-helicity. The correlation function as a function of the wavenumber (decomposed in perpendicular and parallel directions to the mean magnetic field) and of the time lag was directly computed for all the different simulations considered, as well as the spatio-temporal spectra. From the correlation functions, we computed the decorrelation time for each Fourier mode, and we compared it with different theoretical predictions for relevant time scales in the system: the local non-linear time, the random sweeping time and the Alfvénic time. It was observed that time decorrelations are dominated by sweeping effects for low values of the mean magnetic field and of the cross-helicity, while for large values of the mean magnetic field or of the cross-helicity, time decorrelations are controlled by Alfvénic effects even when the Alfvén time is not the fastest time, a new feature when compared with previous studies of spatio-temporal behavior of strong MHD turbulence with zero cross-helicity. In principle, this behavior could be interpreted as a transition towards a regime with weaker non-linearities as the cross-helicity is increased.

However, it should be noted that the spatio-temporal spectra indicate that even in this regime non-linear interactions are relevant: The other main result obtained from our analysis is the finding of a regime in which opposite polarizations $\mathbf{z}^-$ and $\mathbf{z}^+$ fluctuations are generated, and propagate in the same direction due to wave reflections caused by inhomogeneities of the large-scale magnetic field. This is more evident in the spatio-temporal spectra of the Elsässer fields for intermediate values of the background magnetic field (that is, when the uniform and constant component of the large-scale magnetic field is not too strong). A phenomenological analysis based on previous ideas in Zhou and Matthaeus[20] indicates that Alfvénic fluctuations with opposite polarizations can indeed propagate in the same direction and even with the same speed. If the background magnetic field becomes too strong (or if the cross-helicity is close to zero), this effect is no longer observed.

Insofar the results analyzed in this paper confirm previous ideas[11,14,17] that (at least in the strong turbulence regime) the wave picture is not complete enough to describe the system of incompressible MHD. A broad band of fluctuations appear in this system coming from lo-

cal and non-local (sweeping) effects, which bring in dispersion and non-linear effects. Moreover, interesting effects such as wave reflection sum up to the complexity of the system, showing the coexistence of wave and turbulence phenomena even in the simplest case of incompressible MHD. This has important implications for applications such as coronal heating, solar wind acceleration, and particle energization in the interplanetary space. As an example, fluctuations observed in the solar wind, which tend to have the magnetic and the velocity field aligned or anti-aligned (i.e., with different Alfvénic polarizations), cannot always be trivially interpreted as travelling "downstream" or "upstream" the mean magnetic field. Extensions of this study to compressible MHD[31], considering the dependence with the cross-helicity in the flow as well as its interplay with compressible effects, would be an interesting follow up of the present study, and a first step towards a deeper understanding of the role of non-linear effects in the propagation of waves in plasma turbulence.

ACKNOWLEDGMENTS

The authors acknowledge support from PICT Grant No. 2015-3530, PIP Grant No. 11220150100324CO, and UBACyT Grant No. 20020170100508BA.

[1] U. Frisch. *Turbulence: The Legacy of A. N. Kolmogorov*. Cambridge University Press, November 1995.

[2] A. Pouquet, U. Frisch, and J. Léorat. Strong MHD helical turbulence and the nonlinear dynamo effect. *Journal of Fluid Mechanics*, 77(02):321–354, September 1976.

[3] Y. Zhou, W. H. Matthaeus, and P. Dmitruk. Magnetohydrodynamic turbulence and time scales in astrophysical and space plasmas. *Rev. Mod. Phys.*, 76(4):1015–1035, December 2004.

[4] A. Alexakis, P. D. Mininni, and A. Pouquet. Turbulent cascades, transfer, and scale interactions in magnetohydrodynamics. *New J. Phys.*, 9(8):298, 2007.

[5] P. D. Mininni. Scale Interactions in Magnetohydrodynamic Turbulence. *Annual Review of Fluid Mechanics*, 43(1):377–397, 2011.

[6] R. H. Kraichnan. The structure of isotropic turbulence at very high Reynolds numbers. *Journal of Fluid Mechanics*, 5(04):497–543, May 1959.

[7] H. Tennekes. Eulerian and Lagrangian time microscales in isotropic turbulence. *Journal of Fluid Mechanics*, 67(03):561–567, February 1975.

[8] S. Chen and R. Kraichnan. Sweeping decorrelation in isotropic turbulence. *Physics of Fluids A: Fluid Dynamics (1989-1993)*, 1(12):2019–2024, December 1989.

[9] M. Nelkin and M. Tabor. Time correlations and random sweeping in isotropic turbulence. *Physics of Fluids A: Fluid Dynamics (1989-1993)*, 2(1):81–83, January 1990.

[10] W. H. Matthaeus, S. Dasso, J. M. Weygand, M. G. Kivelson, and K. T. Osman. Eulerian Decorrelation of Fluctuations in the Interplanetary Magnetic Field. *ApJ*, 721(1):L10, 2010.

[11] S. Servidio, V. Carbone, P. Dmitruk, and W. H. Matthaeus. Time decorrelation in isotropic magnetohydrodynamic turbulence. *EPL*, 96(5):55003, 2011.

[12] F. Carbone, L. Sorriso-Valvo, C. Versace, G. Strangi, and R. Bartolino. Anisotropy of Spatiotemporal Decorrelation in Electrohydrodynamic Turbulence. *Phys. Rev. Lett.*, 106(11):114502, March 2011.

[13] M Dobrowolny, A Mangeney, and P Veltri. Fully developed anisotropic hydromagnetic turbulence in interplanetary space. *Physical Review Letters*, 45(2):144, 1980.

[14] P. Dmitruk and W. H. Matthaeus. Waves and turbulence in magnetohydrodynamic direct numerical simulations. *Physics of Plasmas (1994-present)*, 16(6):062304, June 2009.

[15] P. Clark di Leoni, P. J. Cobelli, and P. D. Mininni. The spatio-temporal spectrum of turbulent flows. *Eur. Phys. J. E*, 38(12):136, December 2015.

[16] R. Meyrand, K. H. Kiyani, and S. Galtier. Weak magnetohydrodynamic turbulence and intermittency. *Journal of Fluid Mechanics*, 770:R1 (11 pages), May 2015.

[17] Rodrigo Lugones, P Dmitruk, Pablo Daniel Mininni, M Wan, and WH Matthaeus. On the spatio-temporal behavior of magnetohydrodynamic turbulence in a magnetized plasma. *Physics of Plasmas*, 23(11):112304, 2016.

[18] R. Meyrand, S. Galtier, and K. H. Kiyani. Direct Evidence of the Transition from Weak to Strong Magnetohydrodynamic Turbulence. *Phys. Rev. Lett.*, 116(10):105002, March 2016.

[19] William H Matthaeus, Ye Zhou, Gary P Zank, and Sean Oughton. Transport theory and the wkb approximation for interplanetary mhd fluctuations. *Journal of Geophysical Research: Space Physics*, 99(A12):23421–23430, 1994.

[20] Ye Zhou and William H Matthaeus. Remarks on transport theories of interplanetary fluctuations. *Journal of Geophysical Research: Space Physics*, 95(A9):14863–14871, 1990.

[21] M Velli. On the propagation of ideal, linear alfvén waves in radially stratified stellar atmospheres and winds. *Astronomy and Astrophysics*, 270:304–314, 1993.

[22] W. H. Matthaeus, G. P. Zank, S. Oughton, D. J. Mullan, and P. Dmitruk. Coronal Heating by Magnetohydrodynamic Turbulence Driven by Reflected Low-Frequency Waves. *The Astrophysical Journal*, 523(1):L93–L96, September 1999.

[23] P Dmitruk, WH Matthaeus, LJ Milano, S Oughton, DJ Mullan, and GP Zank. Coronal heating distribution due to alfvenic driven magnetohydrodynamic turbulence. In *AGU Spring Meeting Abstracts*, 2001.

[24] W. H. Matthaeus, S. Oughton, and Y. Zhou. Anisotropic magnetohydrodynamic spectral transfer in the diffusion approximation. *Phys. Rev. E*, 79(3):035401, March 2009.

[25] W. Heisenberg. Zur statistischen Theorie der Turbulenz. *Z. Physik*, 124(7-12):628–657, July 1948.

[26] G. Comte-Bellot and S. Corrsin. Simple Eulerian time correlation of full-and narrow-band velocity signals in grid-generated, turbulence. *Journal of Fluid Mechanics*, 48(02):273–337, July 1971.

[27] S. A. Orszag and G. S. Patterson. Numerical Simulation of Three-Dimensional Homogeneous Isotropic Turbulence. *Phys. Rev. Lett.*, 28(2):76–79, January 1972.

[28] P. Clark di Leoni, P. J. Cobelli, P. D. Mininni, P. Dmitruk, and W. H. Matthaeus. Quantification of the strength of inertial waves in a rotating turbulent flow. *Physics of Fluids (1994-present)*, 26(3):035106, March 2014.

[29] D. O. Gómez, P. D. Mininni, and P. Dmitruk. Parallel Simulations in Turbulent MHD. *Phys. Scr.*, 2005(T116):123, 2005.

[30] D. O. Gómez, P. D. Mininni, and P. Dmitruk. MHD simulations and astrophysical applications. *Advances in Space Research*, 35(5):899–907, 2005.

[31] Nahuel Andrés, Patricio Clark Di Leoni, Pablo Daniel Mininni, Pablo Dmitruk, Fouad Sahraoui, and William H Matthaeus. Interplay between alfvén and magnetosonic waves in compressible magnetohydrodynamics turbulence. *Physics of Plasmas*, 24(10):102314, 2017.